Bulletin of the Seismological Society of America, Vol. 72, No. 6, pp. 1881–1902, December 1982

THREE-DIMENSIONAL SIMULATION OF SPONTANEOUS RUPTURE: THE EFFECT OF NONUNIFORM PRESTRESS

By Steven M. Day

ABSTRACT

We use a finite difference method to study crack propagation in a three-dimensional continuum, for conditions of both uniform and nonuniform prestress. The rupture criterion employed satisfies two fundamental physical requirements: it ensures finite stresses in the continuum and finite energy dissipation in crack extension. The finite stress numerical simulations exhibit abrupt jumps in rupture velocity when sharp changes in prestress are encountered on the crack plane, behavior analogous to that predicted theoretically for two-dimensional, singular cracks. For uniform prestress conditions, the slip velocity function is approximately a low-pass filtered version of that of a singular, constant rupture velocity crack. For nonuniform prestress, spatial variations of peak slip velocity are strongly coupled to spatial variations of rupture velocity.

For uniform prestress and low cohesion, rupture velocity is predicted to exceed the *S*-wave velocity in directions for which mode II (inplane) crack motion dominates. A subshear rupture velocity is predicted for directions of predominantly mode III (antiplane) crack motion. Introduction of stress heterogeneities is sufficient, in each of the three cases studied, to reduce average rupture velocity to less than the *S* velocity, but local supershear rupture velocities can still occur in regions of high prestress. Rupture models with significant segments of supershear propagation velocities may be consistent with seismic data for some large earthquakes, even where average rupture velocity can be reliably determined to be subshear.

Introduction

It is generally assumed that earthquake ground motion results from unstable slip accompanying a sudden drop in shear stress on a geologic fault. An important theoretical tool for studying such ground motion has been the so-called "dislocation" earthquake model. In this approach, the earthquake is represented in terms of the displacement discontinuity, or "slip function," on the fault plane. The form of the slip function is generally chosen on an intuitive basis, without rigorous analysis of the time-dependent stresses acting in the focal region.

In contrast to dislocation models, "dynamic" earthquake models are those which take explicit account of the driving (tectonic) and resisting (frictional) stresses in the source region, and derive the resulting slip via the equations of motion. Such earthquake models generally lead to nonlinear, mixed boundary value problems requiring numerical methods for their solution. The three-dimensional case, in particular, presents formidable computational requirements.

In this study, we present numerical solutions for the rupture and slip histories predicted by a dynamic earthquake model. We consider various conditions of both uniform and nonuniform prestress. Our objective is to obtain an improved theoretical understanding of potential rupture propagation effects on earthquake ground motion. The earthquake is modeled as a spontaneously propagating shear crack in a three-dimensional continuum, with rupture growth governed by a slip-weakening failure criterion. The equations of motion are solved by a finite difference method.

A number of studies have treated the three-dimensional dynamic problem of a propagating shear fault with the simplification that rupture velocity is specified *a*

priori rather than being derived from a failure criterion. These results are reviewed by Das (1981) and Day (1982).

Numerical solutions for fixed rupture velocity dynamic faults have satisfactorily quantified some important three-dimensional geometrical effects such as the influence of fault width on the slip function. In the latter reference, for example, closed-form approximations are developed for the dependence of final slip, slip rise time, and slip velocity intensity (i.e., the strength of the crack-edge velocity singularity) on fault width and length. By means of such relationships, the fixed rupture velocity dynamic models help establish physical interpretations for the purely kinematic parameters associated with the more routinely used dislocation earthquake models (e.g., Swanger *et al.*, 1980).

Madariaga's (1977) analysis suggests that changes in rupture velocity of a propagating fault are the predominant source of high-frequency radiation. To gain a physical understanding of unsteady rupture propagation requires a "spontaneous rupture" dynamic model. That is, a failure criterion must be introduced into the numerical simulation so that rupture growth is determined as part of the dynamic solution. Spontaneous rupture dynamic models have been studied in two dimensions, using both analytical and numerical solutions. Freund (1979) provides a good review of this work.

Three-dimensional solutions for spontaneous shear cracks are very limited in number. Numerical solutions have been obtained by Day (1979), using the "slip-weakening" failure criterion (Ida, 1972; Andrews, 1976a), and by Das (1981) and Virieux and Madariaga (1982), using the "critical stress level" criterion (Das and Aki, 1977).

In this paper, we first describe the conceptual and experimental bases for the slip-weakening rupture model and point out some of the uncertainties involved in applying the model to the scale of geologic faulting. In the subsequent section, we apply the rupture model to obtain finite difference solutions for spontaneous rupture in a uniformly prestressed whole-space. Then we turn to the effects of nonuniform prestress. We study finite difference simulations for three particular problems. In two cases, the prestress configuration consists of a single, isolated concentration of high stress on the fault plane. The third case consists of five separate stress concentrations, with intervening lower stress areas.

Our focus in the present paper is on the rupture process itself, particularly the dependence of rupture velocity and slip velocity, respectively, on prestress and fault strength. Our intent is to identify specific phenomena associated with rupture propagation which may be important for defining the seismic radiation. We deliberately treat problems involving only simple geometries, and make no effort to simulate the full range of complexity which might be present in the earth.

An important further step will be to determine how the rupture phenomena identified in this study would be manifested in the radiated seismic signal. The slip histories obtained from the numerical solutions presented here are sufficient to synthesize the radiated wave field, and this issue will be considered in a subsequent report.

Fault Model

The model of faulting employed here follows that described by Day (1982), except that rupture is spontaneous, not prescribed *a priori* as in that study. In particular, we retain the approximation that faulting is confined to a single plane and that the continuum is linearly elastic everywhere outside that plane. In this

model, any inelastic response of the fault zone must be approximated through a (nonlinear) boundary condition on the fault plane. We will use the terms "failure" and "rupture" interchangeably to denote loss of strength of the fault zone, without prejudice as to whether the actual process of faulting in the earth more nearly resembles frictional sliding on a discrete fault plane or fracture of intact rock.

When an abrupt stress drop is imposed on a crack in an otherwise linearly elastic continuum, the stress at the crack edge is singular. As pointed out by Andrews (1976a), this is true even though, in special cases, the traction acting on the crack plane may itself be nonsingular. The basic assumption guiding our construction of a failure criterion is that material strength is finite so that shear stress concentrations near the crack edges must be bounded by some prescribed yield stress. As noted by Andrews, bounded stress must be accompanied by energy absorption at the rupture front as rupture extends.

One way to avoid the stress singularity is to posit a "cohesive zone" just ahead of the crack edge in which slip is resisted by some distribution of cohesive tractions. Ida (1972) introduced the slip-weakening shear-crack model, in which the cohesive

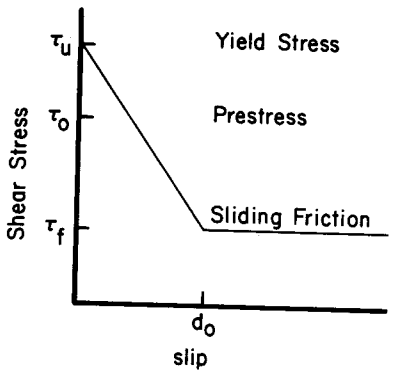

FIG. 1. Sketch of the slip-weakening model. The curve represents the shear stress level on the fault required to sustain sliding, as a function of the slip path length.

traction is assumed to depend only on the amount of slip across the crack. Ida analyzed the steady-state problem of a propagating, antiplane shear crack, for various functional forms of slip weakening. It was demonstrated that this model is equivalent to the Griffith criterion in its prediction of rupture growth, provided the zone over which the cohesive tractions act is small compared with the overall crack dimension. The specific fracture energy of the Griffith criterion was identified with the work done by the cohesive traction.

In this study, we employ the slip-weakening model in the form given by Andrews (1976a), and illustrated in Figure 1, with some obvious generalizations to three dimensions. The shear traction vector τ on the fault plane is limited in magnitude by a finite yield stress, τ_u, which is greater than, or equal to, the initial equilibrium value of traction, τ_0. Slip commences at a point when necessary to prevent the magnitude of τ from exceeding τ_u. This relative displacement is denoted $\boldsymbol{s}$, and has a path length denoted by σ, where σ is given in differential form by $d\sigma^2 = d\boldsymbol{s} \cdot d\boldsymbol{s}$. The slip is assumed to weaken the fault plane at that point, reducing the shear traction required to sustain sliding by an amount proportional to σ. Finally, when σ reaches a critical value, d_0, cohesion is considered to be destroyed, and further sliding occurs at a specified "dynamic friction" level, τ_f.

We will define the dynamic stress drop, $\Delta\tau$, to be the difference between the absolute values of shear prestress and sliding frictional stress,

$$\Delta\tau = \tau_0 - \tau_f. \tag{1}$$

A second important quantity is a dimensionless ratio which Das and Aki (1977) call S, and which is a measure of how near the initial stress field is to failure. This ratio is defined by

$$S = \frac{\tau_u - \tau_0}{\Delta\tau}, \tag{2}$$

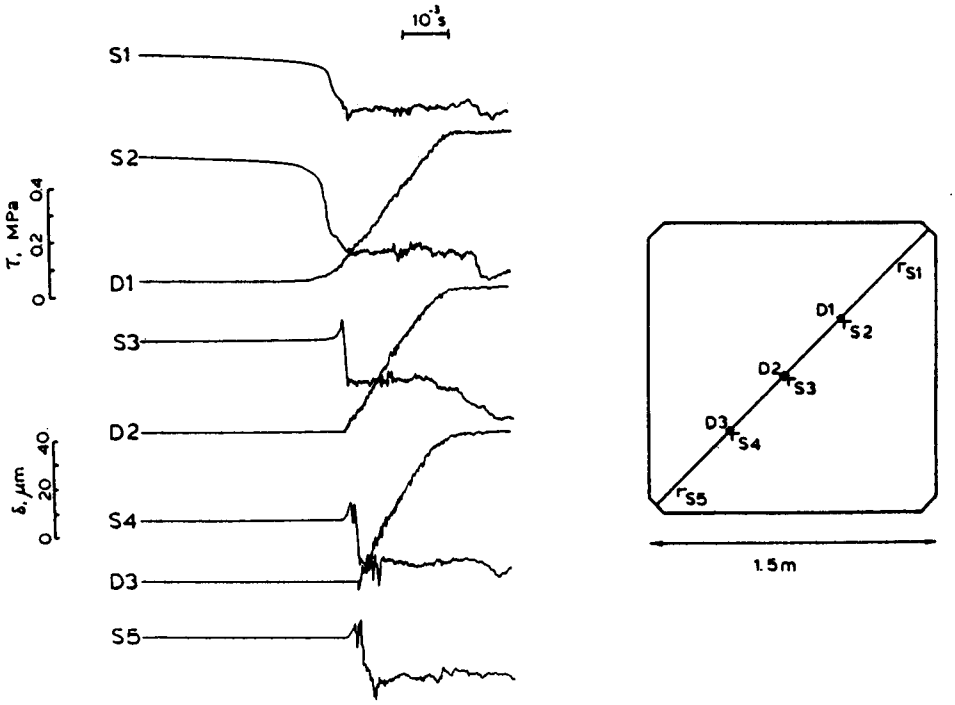

FIG. 2. Laboratory measurements of fault shear stresses and relative displacements, versus time, for an unstable slip event in granite (from Dieterich, 1980).

and $S + 1$ represents the stress change which occurs across the rupture front, normalized to the dynamic stress drop.

This failure model satisfies the requirement that stress be everywhere finite. The energy dissipated in overcoming cohesion, per unit area encompassed by extension of the rupture, is denoted by 2γ. It is given by

$$2\gamma = \tfrac{1}{2}\, d_0(\tau_u - \tau_f). \tag{3}$$

and γ can be interpreted as a specific fracture energy.

Laboratory measurements of rock friction show slip-weakening behavior of this type. Dieterich *et al.* (1978) and Dieterich (1980) have measured time histories of shear stress and slip during unstable slip events induced on lapped sawcuts in large

laboratory samples (granite blocks, with long dimension on the order of 1 m). An example of these observations of unstable slip events, taken from the latter reference, is shown in Figure 2. Dieterich examined in detail the shear stress versus displacement curves for several such events. He finds that the stress drop at the onset of rupture is not instantaneous. Instead, a finite slip of approximately 3 to 5 μm is required before the residual sliding friction level is reached. The intervening stress-displacement behavior is very similar to that assumed in Figure 1 (see, e.g., Figure 6 of Dieterich, 1980). These laboratory results lend support to the simple slip-weakening criterion as a reasonable model for unstable frictional sliding. We will proceed on the hypothesis that unstable frictional sliding, in turn, is a useful analog for natural earthquakes with source dimensions of the order of hundreds to thousands of meters.

From Dieterich's data, reproduced in Figure 2, we can infer a representative value of S. This ratio lies in the range 0.0 to 0.5 for the five stress recordings shown, $S1$ through $S5$. In our numerical experiments with uniform prestress, we will examine

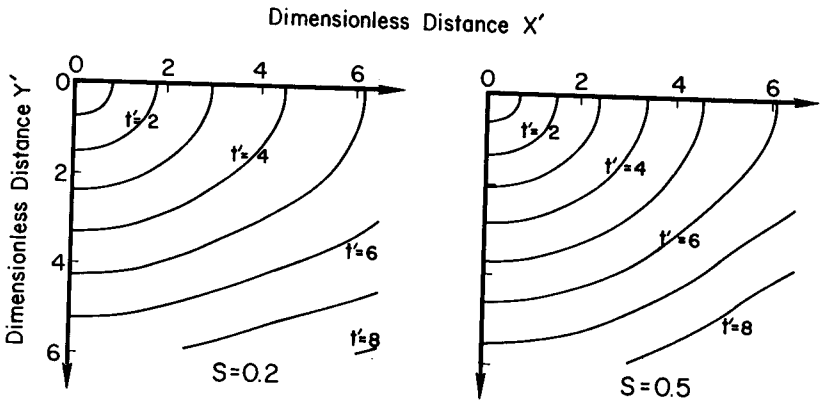

FIG. 3. Rupture front contours, at unit intervals of the dimensionless time, for the case of uniform prestress. The two cases represent numerical simulations performed for $S = 0.2$ and $S = 0.5$, respectively.

rupture propagation for two values of S in this range, $S = 0.2$ and $S = 0.5$. We cannot be sure, of course, that these values are representative of actual earthquake faulting. In fact, the numerical results in the next section suggest that, on the average, cohesive stresses are probably somewhat larger than implied by these values of S.

We will also need an estimate for the fractional stress drop, $\Delta\tau/\tau_0$. Laboratory stick-slip experiments in rock give values of $\Delta\tau/\tau_0$ of a few per cent to a few tens of per cent (e.g., Byerlee, 1967; Scholz *et al.*, 1972; Dieterich *et al.*, 1978). In our numerical simulations with uniform prestress, $\Delta\tau/\tau_0$ will be set to 0.1. Actually, for a given value of $\Delta\tau$, the value of $\Delta\tau/\tau_0$ has very little effect on the dynamic solution; it influences principally the amount of slip which occurs in the direction perpendicular to the prestress direction, and this slip component is usually small in any case. The main importance of estimating $\Delta\tau/\tau_0$, in the context of the slip-weakening model, is to guide our estimation of d_0.

Laboratory results give us few guidelines from which to estimate d_0, apart from the qualitative one that d_0 may be substantially larger for geologic faults than for

laboratory faults since it appears to increase with surface roughness and gouge particle size (Dieterich, 1981). The numerical solutions for uniform stress will be nondimensionalized with respect to d_0. In the nonuniform stress simulations, however, we introduce a length scale into the problem; so we will have to assign numerical values to d_0. For the reason discussed below, we will use values of d_0 several orders of magnitude larger than the laboratory values, which range from roughly 2×10^{-6} to 2×10^{-4} m (Dieterich, 1980).

If we are to retain the analogy to frictional sliding, relatively large values of d_0 appear to be required to prevent those stress components not relieved by slip on the fault from exceeding the failure stress. To see this, we perform a calculation similar

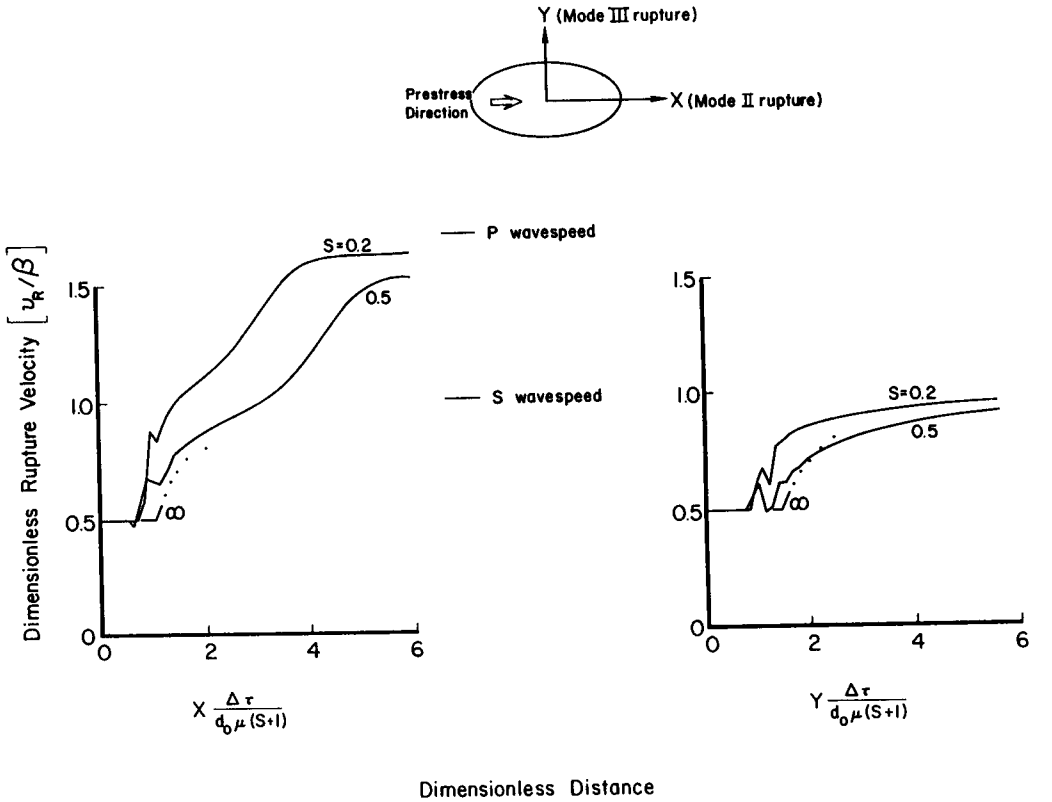

FIG. 4. Rupture velocity as a function of dimensionless distance, for the case of uniform prestress. The solutions are shown along both the x axis (prestress direction) and the y axis. Numerical solutions are given for two finite values of the strength parameter S. Also shown is the analytic solution for the onset of spontaneous rupture in the singular case ($S = \infty$).

to one done by Andrews (1976a). For mode III (antiplane strain) crack propagation, in which the shear stress component τ_{yz} is relieved on the plane y = zero, Ida and Aki (1972) give the following expression for the unrelieved component of shear stress on $y = 0$, τ_{xz}

$$\tau_{xz} = \frac{\mu \dot{s}}{2v_R}, \tag{4}$$

where μ is the shear modulus, v_R is the rupture velocity, and $\dot{s}$ is the slip rate. Ida (1972) obtained a numerical estimate of the peak value of $\dot{s}$ for an antiplane crack in which τ_{yz} is limited by the slip-weakening criterion. His result can be written as

$$\max(\dot{s}) \approx 0.68 \frac{4V^2}{d_0 v_R} \tag{5}$$

where V is the slip velocity intensity for the so-called "macroscopic," or "large-scale" solution. That is, V characterizes the crack-tip velocity for the corresponding

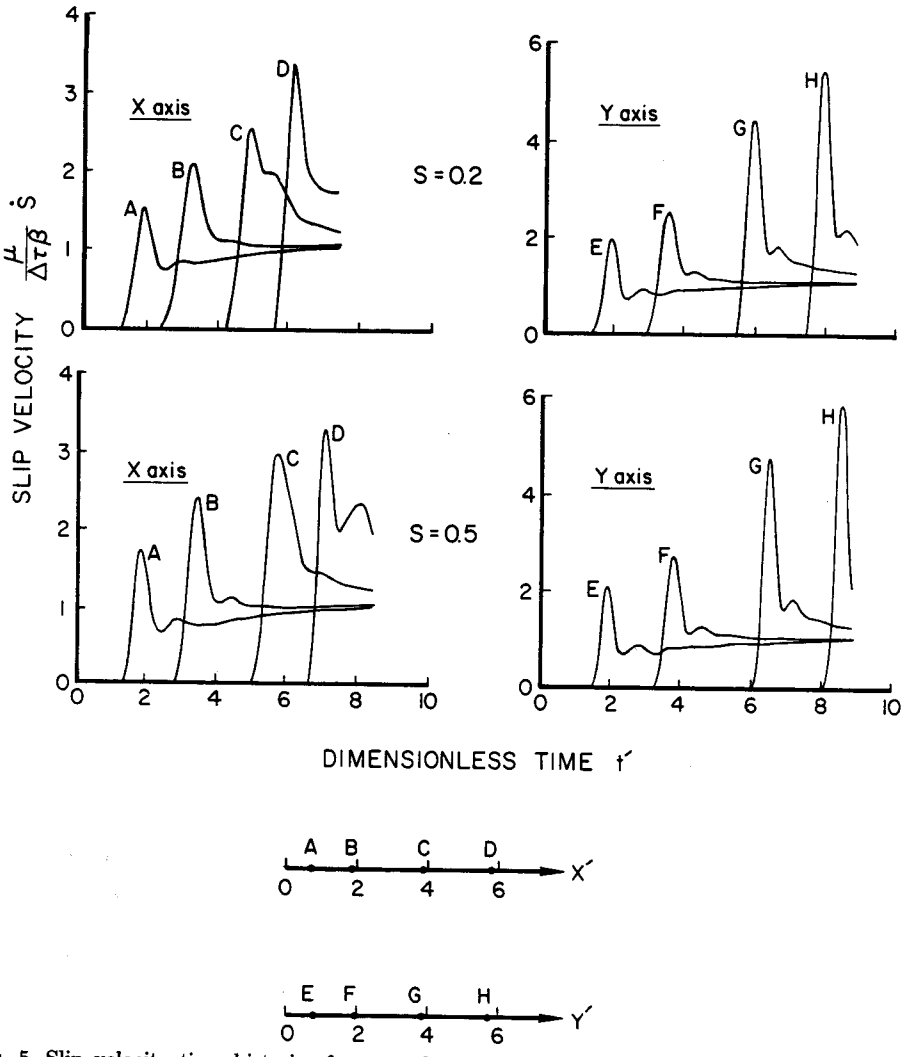

FIG. 5. Slip velocity time histories for several points along the x and y axes, for the numerical simulations with uniform prestress. The time histories have been low-pass filtered, with a nondimensional cutoff period of 0.6.

singular crack problem, and is defined by

$$\dot{s} \sim V\xi^{-1/2},$$

where ξ is distance behind the crack tip, and ξ is small compared to the overall crack length, but still exceeds the length over which the cohesive stresses act.

Although equations (4) and (5) were derived for the antiplane problem, we will assume that they also provide a rough estimate of maximum shear stress in the

general case of a shear crack in three dimensions. Day (1982) determined V numerically for propagating rectangular shear cracks in three dimensions, and found that V is limited by the narrow dimension of the crack, W. Using his approximation for V,

$$V \approx \sqrt{\frac{W}{2}\frac{\Delta\tau}{\mu}}\, v_R,$$

together with equations (4) and (5), we find, very approximately,

$$\text{Maximum shear stress} \approx \frac{W\Delta\tau^2}{\mu d_0}.$$

Therefore, to ensure that the maximum shear stress does not exceed τ_u, it is adequate that d_0 obey approximately

$$d_0 > \frac{W\Delta\tau^2}{\mu \tau_u}. \tag{6}$$

TABLE 1

FAULT PARAMETERS FOR NONUNIFORM PRESTRESS SIMULATIONS

Problem No.	d_0 (m)	τ_u (MPa)	τ_f (MPa)	Max τ_0 (MPa)	Min τ_0 (MPa)
I	0.10	102	90	100	90.0
II	0.10	102	90	100	92.5
III	0.08	102	90	100	92.5

For example, for a fault width of 4 km, a dynamic stress drop of 10 MPa (100 bars), shear modulus of 3.2×10^4 MPa, S of 0.5, and fractional stress drop equal to 0.1, the inequality (6) is satisfied for d_0 of about 0.12 m or greater. This set of parameters would imply a fracture energy γ of about $4.5 \times 10^5\ Jm^{-2}$, which happens to be very close to Aki's (1979) estimate of $4 \times 10^5\ Jm^{-2}$ for the specific fracture energy associated with stopping of rupture during the 1966 Parkfield earthquake.

The above considerations should roughly apply even if we acknowledge that failure is probably not strictly confined to a plane. Then, the interpretation would be that large values of d_0 are necessary in order for the specific fracture energy (which is proportional to d_0 in our model) to adequately simulate energy loss through inelastic work in the continuum. It is obvious, however, that considerable uncertainty exists, both as to the numerical value and physical interpretation of the model parameter d_0.

UNIFORMLY PRESTRESSED FAULT

Problem description. We use the slip-weakening model to simulate spontaneous rupture in a uniform whole-space. The fault occupies the plane $z = 0$ and relieves the xz component of stress. Rupture starts at the origin and grows outward, and the fault slip is symmetric about both the x and y axes. The prestress, τ_0, strength, τ_u, frictional stress, τ_f, and the critical slip, d_0, are all constant on the plane $z = 0$. The continuum is a Poisson solid; i.e., the ratio of the P-wave speed, α, to the S-wave speed, β, equals $\sqrt{3}$. The fractional stress drop, $\Delta\tau/\tau_0$, is 0.1, although variations of

$\Delta\tau/\tau_0$ would have very little effect on the numerical solutions. We will consider two values of S, $S = 0.2$ and $S = 0.5$.

The relevant boundary value problems are solved using a three-dimensional finite difference method. The dynamic solution is explicitly time-stepped, and artificial viscosity is used to suppress any high-frequency oscillations in the solution caused by the numerical dispersion which is intrinsic to discrete numerical methods such as finite difference. As a further precaution, the slip velocity time histories are post-processed with a low-pass filter to remove any significantly dispersed high-frequency components of the solution.

Rupture inception. Once started in a uniform stress field, rupture proceeds spontaneously, without stopping, driven by the dynamic stress concentration at the fault edges. However, some additional mechanism is required to initiate rupture from the equilibrium prestress configuration. We might imagine, e.g., that a relatively small area on the prospective fault plane has been weakened, and that the

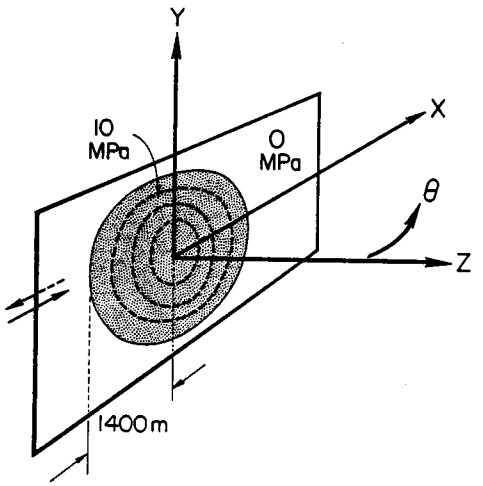

FIG. 6. Fault geometry for nonuniform prestress problem I.

shear stress there falls from τ_0 to τ_f. This initial crack then slides stably under a slowly increasing tectonic load. Eventually, a situation develops which is analogous to the critical crack in elastic fracture mechanics, and accelerating crack growth ensues.

Our interest will be confined to the dynamics of faulting after the onset of instability, and we will not concern ourselves here with the quasi-static processes leading to instability. Instead, we will simply induce an instability artificially, as described later. However, in order to establish a fundamental length scale for the dynamic solution, it is useful to estimate the size of a critical static crack. For this purpose, we assume that the crack is initially circular. We further assume (only for the present purpose, however) that, at the onset of instability, the circular crack initially expands uniformly, retaining circular shape. To estimate the critical radius, r_c, we seek a balance between strain energy release rate and the energy dissipation rate at the crack edge, per unit increase in the crack radius. We start with Neuber's (1937) solution for the static slip on a circular shear crack in a Poisson solid

$$s_\infty(r) = \frac{24}{7\pi}\frac{\Delta\tau}{\mu} r_c \sqrt{1 - \frac{r^2}{r_c^2}}, \tag{7}$$

where s_∞ is the static slip, μ is the shear modulus, β is the shear wave speed, r_c is the crack radius, and r is the distance from the crack center. The total "available" energy, E, is defined as the drop in strain energy due to crack formation minus the work done against friction, and can be calculated from equation (7)

$$E = \frac{8\Delta\tau^2 r_c^3}{7\mu}. \tag{8}$$

The slip-weakening mechanism dissipates energy Σ at the rupture front at the rate

$$\frac{d\Sigma}{dr_c} = \pi\,(S+1)\,d_0 r_c \Delta\tau \tag{9}$$

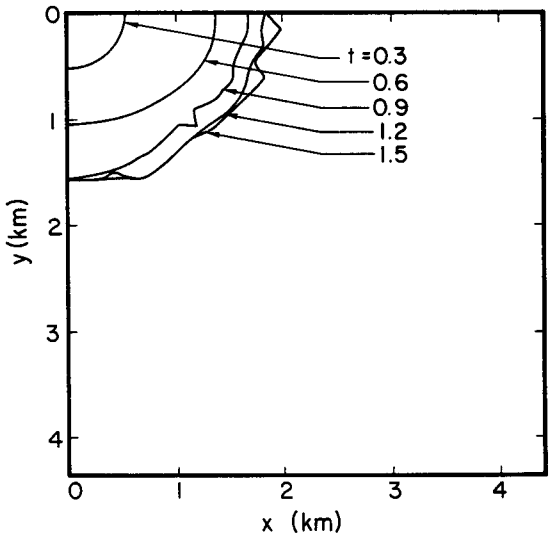

FIG. 7. Rupture front contours obtained from the numerical solution to problem I. The rupture front is shown at 0.3-sec intervals. The fault stops spontaneously after 1.5 sec.

per unit increase in crack radius. The desired estimate of the critical radius is r_c such that E–Σ is stationary, which gives

$$r_c = \frac{7\pi}{24}\frac{\mu(S+1)\,d_o}{\Delta\tau}. \tag{10}$$

For our dynamic simulations, we have induced an instability through the artifice of enforcing, within the focal region, a minimum rupture velocity equal to half the shear speed β (Andrews, 1976b, used a similar method to start plane-strain shear cracks). The choice of this value for minimum rupture velocity is a compromise between approximating quasi-static crack inception (favored by rupture velocity approaching zero) and reducing computation time (favored by a high minimum rupture velocity).

Numerical results for rupture velocity. Because of the spatial uniformity of the problem, there is no intrinsic length scale apart from the critical crack radius [equation (10)]. We will present the numerical results in nondimensional form using

r_c as the fundamental length unit. Since the derivation of r_c is approximate, however, we will ignore the numerical factor $\frac{7\pi}{24}$ in equation (10). Then, distance x and time t, respectively, are given in terms of the nondimensional variables, x' and t', by

$$x = \frac{(S+1)\,\mu d_0}{\Delta\tau} x'$$
$$t = \frac{(S+1)\,\mu d_0}{\Delta\tau\beta} t'. \tag{11}$$

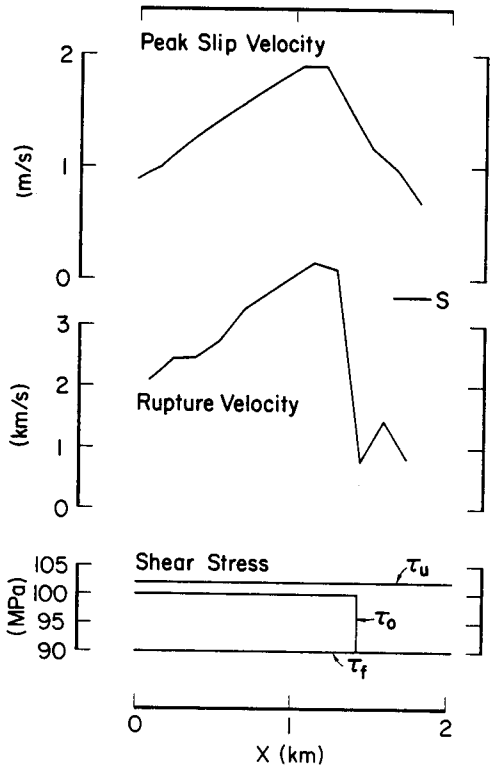

FIG. 8. Rupture velocity and peak slip velocity for problem I, as functions of position along the x axis. Peak slip velocity is obtained from low-pass filtered (5-Hz cutoff) time histories of slip. The S-wave velocity is shown by a horizontal line, indicating that the local rupture velocity is slightly supershear near the edge of the stress concentration.

Figure 3 shows contours of the rupture front at equal intervals of dimensionless time, t', for the two values of S. The rupture front is defined to enclose regions of the fault plane on which the slip has exceeded d_0. For both values of S, rupture propagation is most rapid in the direction of prestress, the x direction, and is least rapid in the y direction; this leads to roughly elliptical rupture fronts. The figure indicates that rupture acceleration is less rapid for the higher strength case, $S = 0.5$, than for $S = 0.2$.

Figure 4 shows rupture velocities obtained from the numerical solutions along the two principal directions. The velocities are shown as functions of hypocentral distance, for both values of S. The initial, flat parts of the curves represent the minimum rupture velocity, $0.5\,\beta$. As the minimum is exceeded, rapid acceleration of

the rupture front occurs. This begins on the x axis (prestress direction) at dimensionless distance of about 0.7, and begins at a slightly greater distance along the y axis.

In the y direction, the rupture velocity smoothly approaches the shear wave velocity; for $S = 0.2$, the rupture velocity reaches 0.95 β by the time the fault has propagated a dimensionless distance of about five. Increasing the strength increases the distance at which a given rupture velocity is achieved, as shown by the curve for $S = 0.5$.

In the x direction, acceleration is more rapid than in the y direction; for $S = 0.2$, the rupture reaches the shear wave velocity at $x' \approx 1.5$. For $S = 0.5$, the shear wave velocity is reached at $x' \approx 3.0$. The rupture velocity then levels off somewhat, before accelerating rapidly again toward the P-wave velocity, α. For $S = 0.2$, the rupture velocity reaches 0.9 α at $x' \approx 3.5$. The leveling off of the rupture velocity near the shear wave velocity is more pronounced for $S = 0.5$, and the acceleration toward the P velocity occurs at greater distance.

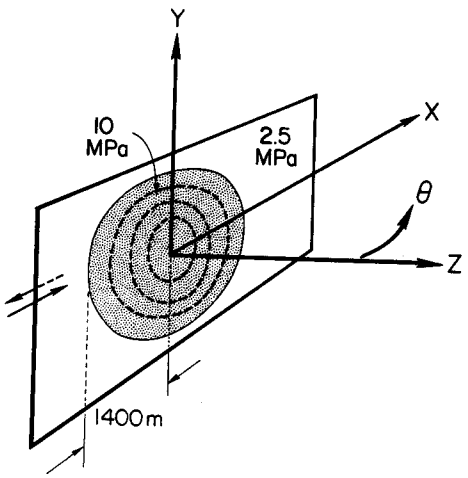

FIG. 9. Fault geometry for nonuniform prestress, problem II.

Also indicated in Figure 4 are the distances along the x and y axes, respectively, at which a singular crack (i.e., the case $S = \infty$), driven at $v_R = 0.5\ \beta$, first begins to accelerate spontaneously. These values are obtained analytically, using standard results for the energy release rate, G, at the edge of a circular crack growing at constant velocity (e.g., Richards, 1976). The energy release rate is a known function of crack radius, rupture velocity, and position on the rupture front; we simply equate G to twice the specific fracture energy, set the rupture velocity to 0.5 β, and solve for crack radius. As was the case for the two numerical solutions for finite S, the singular rupture front begins accelerating first along the x axis (the prestress direction), and last along the y axis.

Once the crack starts accelerating, the analytic results for $S = \infty$ no longer apply. The dotted lines suggest the expected behavior of the singular crack, based on the approximation of using the self-similar circular crack solution for G after the onset of accelerating rupture.

The most important aspect of Figures 3 and 4 is the prediction of rupture velocities exceeding the shear wave velocity for propagation in the direction of mode II crack extension (x axis). On the other hand, rupture remains subshear in the direction of

purely mode III crack propagation (the y direction). Das (1981) has obtained similar results using the critical stress level criterion of failure.

The result that the mode III rupture is subshear, but approaches the S-wave velocity asymptotically, agrees with two-dimensional analytical solutions for mode III cracks (e.g., Kostrov, 1966). The prediction of supershear rupture in the direction of prestress, for both $S = 0.2$ and $S = 0.5$, is in agreement with Burridge's (1973) two-dimensional analysis of mode II rupture propagation for a finite stress rupture criterion. The two-dimensional numerical solutions of Das and Aki (1977) and Andrews (1976b) also yield supershear rupture velocities for values of S similar to those used here. Those studies have established, however, that for values of S exceeding approximately 1.63, mode II rupture propagation is subshear. This result is expected to govern the three-dimensional solution, as well; so for substantially higher fault strength relative to $\Delta\tau$, rupture velocity is expected to be subshear in all directions.

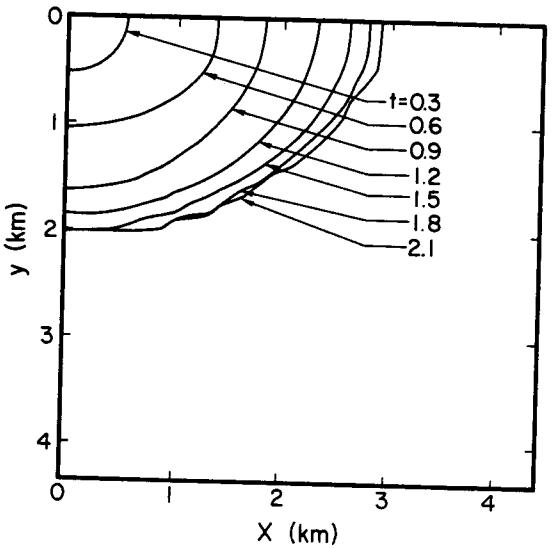

FIG. 10. Rupture front contours obtained from the numerical solution to problem II, shown at 0.3-sec intervals. Fault growth stops spontaneously at approximately 2.1 sec.

Earlier, we discussed some observations made by Dieterich of unstable slip events in granite blocks with dimensions of the order of 1 m. Typical fault parameters observed in these experiments are (see Figure 2) $\Delta\tau \approx 0.2$ MPa, $S \approx 0.5$, and $d_0 \approx 3 \times 10^{-6}$ m. Then, assuming $\mu \approx 3 \times 10^4$ MPa for granite, we find that a hypocentral distance of 1 m corresponds to a dimensionless distance x' of about 1.5. From Figure 4, we see that this is well within the range of subshear rupture velocity for $S = 0.5$. Thus, the numerical solutions indicate that rupture velocities will usually be subshear for similar experiments on this scale. This prediction is sensitive to the value of S, however; for $S = 0.2$, e.g., a 1-m distance corresponds to $x' = 1.8$, which, according to Figure 4, is close to the distance for transition to supershear rupture, for this value of S. It is conceivable, then, that rupture velocity measurements on this length scale will occasionally exceed β, for similarly prepared fault surfaces.

Numerical results for slip velocity. Normalized slip velocities along the x and y axes are shown in Figure 5. These have been low-pass filtered to attenuate Fourier components with (nondimensional) periods shorter than about 0.6. The figure shows that the peak (low-passed) slip velocity increases with focal distance. The increase

appears to be similar in form to the $\sqrt{r}$ increase found analytically for circular, fixed rupture velocity models (Kostrov, 1964). Peak slip velocity, at a given focal distance, is higher on the y axis than on the x axis. This azimuthal variation is qualitatively explained by the Burridge and Willis (1969) solution for the slip s on a self-similar, expanding elliptical crack

$$s = C\frac{\Delta\tau\beta}{\mu}\left(t^2 - \frac{x^2}{v_x^2} - \frac{y^2}{v_y^2}\right)^{\frac{1}{2}} H\left(t^2 - \frac{x^2}{v_x^2} - \frac{y^2}{v_y^2}\right) \tag{12}$$

where C is a constant and v_x and v_y are the rupture velocities in the x and y directions, respectively. This expression predicts that peak (low-passed) slip velocity,

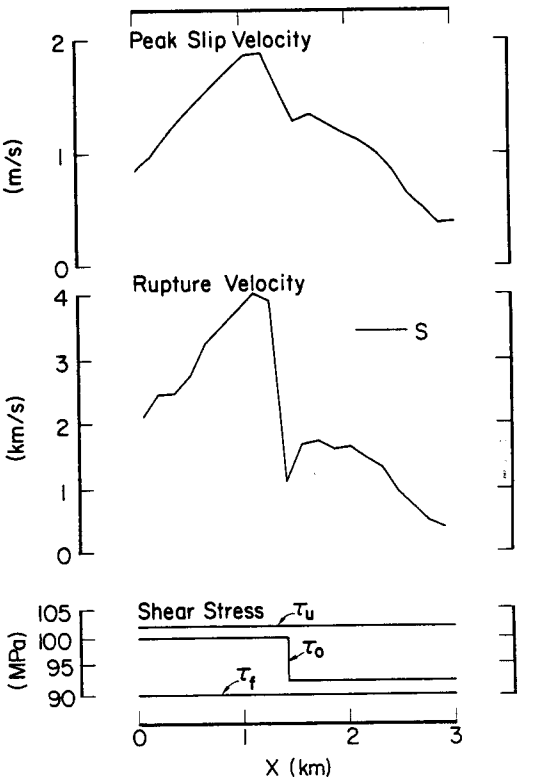

FIG. 11. Rupture velocity and peak slip velocity for problem II, as functions of position along the x axis. Peak slip velocity is obtained from low-passed (5-Hz cutoff) time histories.

on the y axis will approach $(v_x/v_y)^{\frac{1}{2}}$ times the peak slip velocity at the same focal distance on the x axis. At $x' = 5.7$, this accounts for about half the observed difference in peak velocity between the two azimuths. The discrepancy is not surprising, considering that equation (12) strictly applies only to singular cracks and for constant rupture velocities, with v_x less than the Rayleigh wave velocity and v_y less than the shear velocity.

The overall shapes of the slip velocity curves are similar to those for the self-similar solution [equation (12)]. That is, they are roughly low-pass filtered, square root singularities. In fact, the peak slip velocities in Figure 5 are very close to what one would predict from low-pass filtering the self-similar solution (which has singular stress) using the same short-period cutoff that was applied to our numerical

solutions. The finite stress condition incorporated into the numerical solution apparently does not substantially reduce peak velocity, relative to singular-stress crack solutions, within the frequency band preserved by the present numerical solutions. Scaled to $\Delta\tau = 10$ MPa, $\mu = 3.24 \times 10^4$ MPa, $\beta = 3.46$ km/sec, and $(S + 1)d_0 = 0.12$ m, the upper frequency cutoff for these calculations would correspond to about 15 Hz, and the maximum hypocentral distance represented in Figure 5 would correspond to about 2.25 km.

These results show that the expression $(\tau_u - \tau_f)\beta/\mu$ does not necessarily provide a good estimate of peak slip velocity, as has been hypothesized previously (e.g., Del Mar Technical Associates, 1978). Figure 5 shows peak slip velocities as high as five times this estimate, and these must be interpreted as lower bounds since the computed velocities have been low-pass filtered.

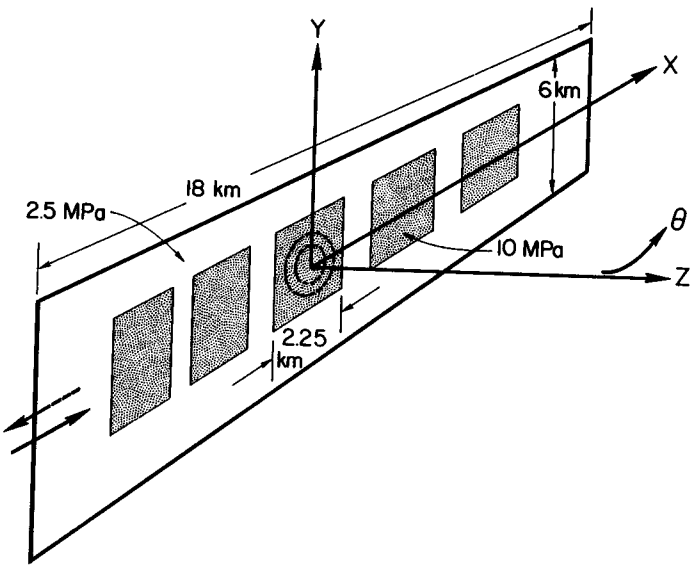

FIG. 12. Fault geometry for nonuniform prestress, problem III.

FAULTS WITH NONUNIFORM PRESTRESS

Introduction. There is growing evidence that spatially inhomogeneous stress changes are a prevalent feature of shallow-focus earthquakes (e.g., Hanks, 1974; Kanamori and Stewart, 1978; Hartzell and Brune, 1979; Bache *et al.*, 1980). Such variations in stress drop, plus the likely variability of frictional strength along faults, may be expected to give rise to irregularities in rupture velocity. Madariaga's (1977) analysis suggests that such rupture velocity variations may be the predominant source of high-frequency radiation from propagating faults. Clearly, it is important to improve our understanding of rupture propagation and its relationship to non-uniformities in the stress field.

In this section, we describe numerical simulations of spontaneous rupture propagation in the presence of localized stress concentrations. Three particular problems are considered. In two cases, the prestress configuration consists of a single, isolated concentration of high shear stress on the fault plane. In both cases, the high-stress patch is embedded in a lower regional stress field. The third case consists of an array of five separate stress concentrations with intervening lower stress zones.

The fault parameters used in the three simulations are given in Table 1. The strength, τ_u, sliding friction τ_f, and critical slip, d_0, are all held constant; only variations of τ_0 are considered. The elastic properties, for all three simulations, are $\alpha = 6.0$ km/sec, $\beta = 3.46$ km/sec, and $\mu = 3.24 \times 10^4$ MPa. In each case, rupture is induced in a high-stress region centered at the origin. The fault then propagates in the $z = 0$ plane, and relieves the x, z stress component. In problems I and II, rupture growth was permitted to stop spontaneously. In problem III, rupture growth decelerated considerably as it progressed into the low-stressed region, but still reached prespecified strength barriers which delimited a 6 km × 18 km rectangular region.

Problem I. Figure 6 shows the geometry for problem I. The high-stress patch ($\Delta\tau = 10$ MPa) is circular, with a radius of 1400 m. Outside this radius, the fault plane is uniformly prestressed at the sliding friction level ($\Delta\tau = 0$).

Figure 7 shows rupture-front contours at 0.3-sec intervals of time. The rupture accelerates rapidly over the prestressed patch, then abruptly decelerates as it breaks into the zero stress-drop region. In the y direction, deceleration is very abrupt, and the fault penetrates only about 150 m beyond the edge of the stress concentration. In the x direction, however, the fault penetrates about 500 m into the low-stress region. After 1.5 sec, rupture growth has ceased.

Figure 8 shows both peak slip velocity (low-passed, 5-Hz cutoff) and rupture velocity along the x axis. Rupture velocity accelerates rapidly throughout the stress concentration as we would predict on the basis of the uniform prestress solution. The shear wave velocity is reached at a hypocentral distance of about 800 m, and rupture velocity is then supershear until reaching the edge of the stress concentration. When the fault breaks into the lower stress region, rupture velocity drops immediately to about 1 km/sec, and rupture growth finally stops spontaneously. The gradual stopping of rupture in a region of zero dynamic stress drop is in qualitative agreement with the predictions of Husseini *et al.* (1975), which were based on an antiplane strain crack model.

It is known, from the analytical results of Eshelby (1969), e.g., that crack edges have no inertia, in the case of singular cracks. That is, rupture velocity responds instantaneously to changes in driving stress. The rupture velocity drops abruptly in our numerical solution as well, after rupturing through the stress concentration. Thus, the finite stress numerical fault model exhibits a lack of inertia similar to that predicted by classical fracture mechanics.

The rupture velocity given in Figure 8 is the local, or "tangent," rupture velocity. That is, it is obtained from the gradient of rupture arrival time. While the tangent rupture velocity exceeds the shear velocity over a significant area of the fault, the average, or "secant," rupture velocity is always subshear in this problem. That is, at any point along the x axis, the hypocentral distance divided by rupture arrival time is less than β for this simulation.

Peak slip velocity roughly parallels the shape of the rupture velocity curve in Figure 8. The initial increase in peak slip velocity with hypocentral distance is expected from our results for the uniform prestress problem. When the rupture velocity decelerates after breaking through the stress concentration, the peak slip velocity also decreases.

Problem II. This case, sketched in Figure 9, differs from the previous one only in having a nonzero dynamic stress drop ($\Delta\tau = 2.5$ MPa) outside the area of stress concentration ($\Delta\tau = 10$ MPa). Figure 10 shows rupture front contours for this case.

Fault growth again stops spontaneously in this case. This spontaneous arrest of rupture occurs in spite of the fact that the prestress everywhere exceeds dynamic friction. As in the previous case, rupture growth decelerates outside the stress concentration, but overshoots further into the lower stress region than was the case in problem I. The overshoot distance is 600 m in the y direction and 1500 m in the x direction, compared to the stress concentration radius of 1400 m.

Rupture velocity and peak slip velocity along the x axis are shown in Figure 11. Local rupture velocity is supershear near the edge of the stress concentration, peaking at about 4 km/sec, and drops abruptly to about 1 km/sec after breaking through the stress concentration. It then recovers to about 1.7 km/sec before smoothly decelerating to zero. Secant rupture velocity is everywhere subshear. The peak slip velocity mirrors this behavior of the local rupture velocity, again demonstrating the strong linkage between the two quantities.

Problem III. The problem geometry for this case is sketched in Figure 12. Each of the five high-stress areas ($\Delta\tau$ = 10 MPa) is square, with dimension 2250 m, and they are symmetrically disposed about the hypocenter. The remainder of the plane is low-stressed ($\Delta\tau$ = 2.5 MPa), and each low-stress area between stress concentrations is 1050 m in width.

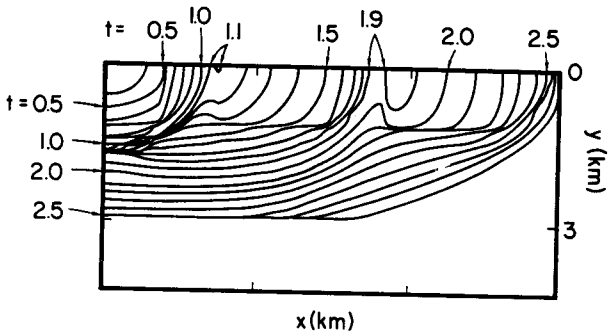

FIG. 13. Rupture front contours obtained from the numerical solution to problem III. Rupture front is shown at 0.1-sec intervals. Contours at 1.1 and 1.9 sec indicate that the rupture has "jumped," with the slipping surface becoming temporarily multiply connected. Fault growth beyond x = 9 km and y = 3 km has been artificially inhibited by a strength barrier.

Figure 13 shows the rupture front contours at 0.1-sec intervals. A fairly complex pattern of rupture emerges. Along the y axis, e.g., rupture stops shortly after 1 sec. As rupture advances on the other parts of the fault plane, however, the stress concentration along the y axis increases, causing rupture propagation to recommence at about 1.8 sec. Along the x axis, rupture accelerates rapidly as it breaks each high-stress patch, and decelerates between patches. At 1.1 sec, and then again at 1.9 sec, the rupture front "jumps," leaving unbroken areas behind, which subsequently break.

Figure 14 shows the peak slip velocities and rupture velocities along the x axis. The close relationship between maximum slip velocity and rupture velocity is especially evident here. The dashed portions of the rupture velocity curve represent regions that ruptured out of sequence as the rupture front jumped ahead to a high-stress patch.

We note that apparent local rupture velocities in excess of the P-wave velocity occur at the edges of the stress concentrations. Of course, the secant rupture velocity (hypocentral distance divided by rupture travel time) is everywhere less than the P-

wave speed, as required by causality. On the other hand, the secant rupture velocity does slightly exceed the S-wave velocity at some intermediate points along the x axis. Over the entire fault length, however, the secant rupture velocity is slightly subshear, equaling approximately 0.95 β.

This behavior is shown another way in Figure 15, which is a plot of distance versus time of rupture along the x axis. The points labeled A and B in this figure illustrate typical positions on the x axis at which tangent rupture velocity is supershear while secant rupture velocity is subshear. At Point A, e.g., the tangent rupture velocity lies between the S- and P-wave velocities, while the secant rupture

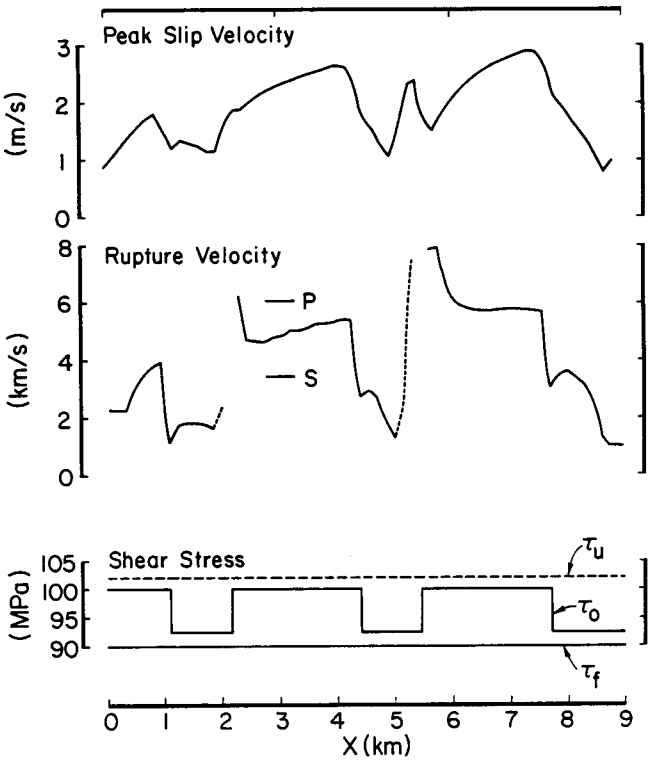

FIG. 14. Rupture velocity and peak slip velocity for problem III, as functions of position along the x axis. Peak slip velocity is obtained from low-passed (5 Hz) time histories. Dashed parts of the rupture velocity curve indicate regions which ruptured out of sequence. For example, rupture occurred at $x = 5.6$ km while the region between 5.0 and 5.6 km was still intact. The linkage between rupture velocity and peak slip velocity is particularly evident in this figure. Note that it is "local" rupture velocity which is plotted—i.e., the derivative of the rupture arrival time curve. Causality is not violated by those portions of the curve which exceed the P-wave velocity.

velocity ($\tilde{v}_R$) is about 80 per cent of the S-wave velocity. At point B, the tangent rupture velocity exceeds the P-wave velocity, while the secant rupture velocity is just over 90 per cent of the S-wave velocity.

The mean value of the dynamic stress drop over the entire 6 × 18 km fault in problem III is about 4.2 MPa. We have defined S for the uniform stress case as the ratio of the cohesive stress ($\tau_u - \tau_0$) to the dynamic stress drop $\Delta\tau$; if we take the ratio of spatial averages of these quantities for the nonuniform stresses of problem III, we get a value of about 1.8. This value is considerably higher than the values for S of 0.2 and 0.5 used in the uniform prestress simulations. As a result, the average rupture velocity has been reduced from well above the shear wave speed for the

uniform stress case to about 5 per cent below the shear wave speed for the nonuniform prestress case. This result can be compared with the theoretical results cited earlier which predict subshear rupture velocity when S exceeds 1.63. It is interesting that the theoretical predictions, which were based on two-dimensional formulations and uniform stress conditions, are in reasonable accord with the gross average behavior of the three-dimensional, nonuniform stress model.

Discussion

We have used a finite difference method to study crack propagation in a three-dimensional continuum, for conditions of both uniform and nonuniform prestress. The model of rupture which was employed satisfies two fundamental physical requirements: it ensures finite stresses in the continuum, and it dissipates energy in the course of crack extension. Furthermore, the rupture model agrees reasonably

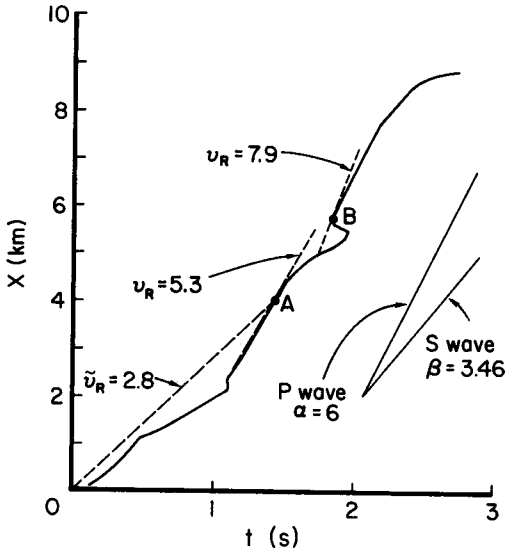

Fig. 15. Distance versus time of rupture along the x axis, for problem III. Point A is a typical point at which the local, or "tangent" rupture velocity v_R exceeds the S-wave velocity, while the average, or "secant" rupture velocity $\tilde{v}_R$ is subshear. Point B represents a point at which the tangent rupture velocity exceeds the P-wave velocity.

well with available laboratory measurements of unstable slip events although scaling of the model parameters to natural earthquakes presents large uncertainties.

In some respects, the behavior of our three-dimensional finite stress numerical simulations resembles that predicted by two-dimensional singular-stress crack models. We observe an abrupt jump in rupture velocity after rupture of a stress concentration, for example, which agrees with the prediction of the singular theory that crack edges lack inertia (Eshelby, 1969). When the dynamic stress drop outside the stress concentration was increased from 0 (problem I) to 2.5 MPa (problem II), the magnitude of the rupture velocity jump diminished slightly, but a finite jump still occurred instantaneously (within the resolution of the numerical solution).

Also foreshadowed by classical fracture mechanics, at least qualitatively, is the strong coupling which we find between rupture velocity and peak slip velocity for the nonuniformly prestressed fault simulations. Analytic solutions (e.g., Freund, 1979) for the elastic field in the vicinity of a propagating crack-tip singularity give

a slip velocity singularity whose intensity is proportional to two factors. The first of these is a functional of the whole rupture history of the crack, and can generally be found only from numerical solutions similar to ours; the second factor, however, increases monotonically with the instantaneous rupture velocity.

In other respects, the behavior of our finite stress numerical simulations is quite different from the behavior of the singular models. An important result to emerge from this and earlier theoretical studies of finite stress shear crack propagation (e.g., Burridge, 1973; Andrews, 1976b; Das and Aki, 1977; Burridge *et al.*, 1979) is the recognition that rupture velocities in excess of the shear wave velocity may be possible when cohesive stresses are sufficiently low. In this study, we have established the applicability of the earlier two-dimensional results to the three-dimensional problem of mixed-mode shear crack propagation. Specifically, supershear rupture velocity is predicted for low-cohesion cracks in directions for which mode II (inplane) crack motion dominates, while subshear velocity is predicted for directions of predominantly mode III (antiplane) crack motion. Das (1981) has obtained a similar result using a different finite stress rupture criterion (the "critical stress level" criterion) and a different numerical method (the boundary integral equation method).

The theoretical work cited above has demonstrated that rupture velocity becomes subshear if the cohesive stress is sufficiently high, i.e., if the dimensionless strength parameter S defined in the text is less than about 1.6. The numerical results presented here demonstrate that average rupture velocity can be reduced to the subshear level by another mechanism as well—the introduction of stress heterogeneities. Furthermore, segments of a fault can rupture at supershear velocity while the average rupture velocity remains subshear. The latter phenomenon was observed in all three of the nonuniform prestress simulations studied.

The numerical results indicate that the possibility of supershear rupture velocity in rock depends on how near the average prestress is to some "failure" stress (which need not be identified with the laboratory strength as measured on small, homogeneous samples of intact rock). Thus, detailed study of rupture propagation velocity and its spatial variability, for a given event, could provide important information on the stress levels acting in the fault zone immediately prior to failure. Several studies have inferred supershear rupture velocities for earthquakes (e.g., Kanamori, 1970; Douglas *et al.*, 1981). These results may be evidence for prestress levels relatively close to failure. Supershear rupture velocities have also been reported for laboratory stick-slip experiments (e.g., Wu *et al.*, 1972; Johnson *et al.*, 1973). In the laboratory studies cited, stick slip was preceded by stable sliding; it may be that the occurrences of supershear rupture velocity reflect a weakened state associated with this stable sliding phase, rather than reflecting the static strength of the fault. On the other hand, Das and Scholz (1981) have cited evidence from earthquake aftershock occurrences, for several events, which suggests the presence of stress levels very close to failure even off the plane of main shock faulting.

Most seismic studies of rupture velocity only estimate its average value. Thus, it is possible that a rupture mechanism analogous to our problem III simulation occurs commonly in nature. That is, some fault segments in large earthquakes may rupture at supershear velocities, even though most reported rupture velocity determinations are less than the shear wave velocity (e.g., Geller, 1976). In fact, Wu and Kanamori (1973) prefer such a mechanism for the 1965 Rat Island earthquake. They infer from seismic surface wave observations that the event had an average rupture velocity of 4 km/sec. At the same time, their analysis of seismic body waves led to a multiple

event interpretation; the inferred rupture velocities for the individual subevents were in the range 5.1 to 6.7 km/sec, values approaching the *P*-wave velocity. Actually, our numerical simulations show that even supersonic (greater than the *P* velocity) rupture velocities may be physically admissible for individual subevents of an earthquake, even though causality demands that its average rupture velocity be subsonic.

Even the relatively simple prestress configurations studied here result in fairly complex rupture histories. An important further step will be to examine their effect on the radiated seismic signal. The radiated wave field can be synthesized using the slip histories obtained from these numerical simulations, and this issue will be considered in a subsequent study.

Acknowledgments

I wish to thank J. B. Minster, J. L. Stevens, and H. J. Swanger for their critical reviews of the manuscript, and K. Aki and J. D. Luco for their helpful critiques of an earlier report on this work. I also thank J. H. Dieterich for permission to reproduce Figure 2. The finite difference computations were done on the ILLIAC IV computer at NASA/Ames Research Center, and programming support at NASA/Ames was directed by S. Biester. This work was supported by the Nuclear Regulatory Commission and by the Defense Advanced Research Projects Agency under Contract F49620-81-C-0094 monitored by the Air Force Office of Scientific Research.

References

Aki, K. (1979). Characterization of barriers on an earthquake fault, *J. Geophys. Res.* **84,** 6140–6148.

Andrews, D. J. (1976a). Rupture propagation with finite stress in antiplane strain, *J. Geophys. Res.* **81,** 3575–3582.

Andrews, D. J. (1976b). Rupture velocity of plane strain shear cracks, *J. Geophys. Res.* **81,** 5479–5687.

Bache, T. C., D. G. Lambert, and T. G. Barker (1980). A source model for the March 28, 1975 Pocatello Valley earthquake from time-domain modeling of teleseismic *P*-waves, *Bull. Seism. Soc. Am.* **70,** 405–418.

Burridge, R. (1973). Admissible speeds for plane-strain self-similar shear cracks with friction but lacking cohesion, *Geophys. J.* **35,** 439–455.

Burridge, R. and J. R. Willis (1969). The self-similar problem of the expanding elliptical crack in an anisotropic solid, *Proc. Camb. Phil. Soc.* **66,** 443–468.

Burridge, R., G. Conn, and L. B. Freund (1979). The stability of a rapid mode II shear crack with finite cohesive traction, *J. Geophys. Res.* **85,** 2210–2222.

Byerlee, J. D. (1967). Frictional characteristics of granite under high confining pressures, *J. Geophys. Res.* **72,** 3639–3648.

Das, S. (1981). Three-dimensional spontaneous rupture propagation and implications for the earthquake source mechanism, *Geophys. J.* **67,** 375–393.

Das, S. and K. Aki (1977). A numerical study of two-dimensional spontaneous rupture propagation, *Geophys. J.* **50,** 643–668.

Das, S. and C. H. Scholz (1981). Off-fault aftershock clusters caused by shear stress increase, *Bull. Seism. Soc. Am.* **71,** 1669–1675.

Day, S. M. (1979). Three-dimensional finite difference simulation of fault dynamics, Final Report SSS-R-80-4295, Systems, Science and Software, La Jolla, California.

Day, S. M. (1982). Three-dimensional finite difference simulation of fault dynamics: rectangular faults with fixed rupture velocity, *Bull. Seism. Soc. Am.* **72,** 705–727.

Del Mar Technical Associates (1978). Simulation of earthquake ground motions for San Onofre Nuclear Generating Station Unit 1, Final report for Southern California Edison Company (submitted for review to the Nuclear Regulatory Commission).

Dieterich, J. H. (1980). Experimental and model study of fault constitutive properties, in *Solid Earth Geophysics and Geotechnology,* AMD-Vol. 42, S. Nemat Nasser, Editor, American Society of Mechanical Engineers, New York.

Dieterich, J. H. (1981). Constitutive properties of faults with simulated gouge, *Geophysical Monograph Series* (J. Handin Festschrift), American Geophysical Union.

Dieterich, J. H., D. W. Barber, G. Conrad and Q. A. Gordon (1978). Preseismic slip in a large scale friction experiment, *Proceedings of the 19th U.S. Rock Mechanics Symposium,* Mackay School of

Mines, University of Nevada, Reno.

Douglas, A., J. A. Hudson, and P. D. Marshall (1981). Earthquake seismograms that show Doppler effects due to crack propagation, *Geophys. J.* **64,** 163–185.

Eshelby, J. D. (1969). The elastic field of a crack extending non-uniformly under general anti-plane loading, *J. Mech. Phys. Solids* **17,** 177–199.

Freund, L. B. (1979). The mechanics of dynamic shear crack propagation, *J. Geophys. Res.* **84,** 2199–2209.

Geller, R. J. (1976). Scaling relations for earthquake source parameters and magnitudes, *Bull. Seism. Soc. Am.* **66,** 1501–1523.

Hanks, T. C. (1974). The faulting mechanism of the San Fernando earthquake, *J. Geophys. Res.* **79,** 1215–1229.

Hartzell, S. H. and J. N. Brune (1979). The Horse Canyon earthquake of August 2, 1975—Two-stage stress-release process in a strike-slip earthquake, *Bull. Seism. Soc. Am.* **69,** 1161–1173.

Husseini, M. I., D. B. Jovanovich, M. R. Randall, and L. B. Freund (1975). The fracture energy of earthquakes, *Geophys. J.* **43,** 367–385.

Ida, Y. (1972). Cohesive force across the tip of longitudinal-shear crack and Griffith's specific surface energy, *J. Geophys. Res.* **77,** 3796–3805.

Ida, Y. and K. Aki (1972). Seismic source time function of propagating longitudinal-shear cracks, *J. Geophys. Res.* **77,** 2034–2044.

Johnson, T., F. T. Wu, and C. H. Scholz (1973). Source parameters for stick-slip and for earthquakes, *Science* **179,** 278–280.

Kanamori, H. (1970). Synthesis of long-period surface waves and its application to earthquake source studies—Kurile Islands earthquake of October 13, 1963, *J. Geophys. Res.* **75,** 5011–5027.

Kanamori, H. and G. S. Stewart (1978). Seismological aspects of the Guatemala earthquake of February 4, 1976, *J. Geophys. Res.* **83,** 3427–3434.

Kostrov, B. V. (1964). Self-similar problems of propagation of shear cracks, *J. Appl. Math. Mech.* **28,** 1077–1087.

Kostrov, B. V. (1966). Unsteady propagation of longitudinal shear cracks, *J. Appl. Math. Mech.* **30,** 1241–1248.

Madariaga, R. (1977). High-frequency radiation from crack (stress-drop) models of earthquake faulting, *Geophys. J.* **51,** 625–651.

Neuber, H. (1937). *Kerbspannungslehre*, Springer-Verlag, Berlin; Theory of notch stresses: principles for exact calculation of strength with reference to structural form and material, the Office of Technical Information, AEC-tr-4547, 1958 (English translation).

Richards, P. G. (1976). Dynamic motions near an earthquake fault: a three-dimensional solution, *Bull. Seism. Soc. Am.* **66,** 1–32.

Scholz, C. H., P. Molnar, and T. Johnson (1972). Detailed studies of frictional sliding of granite and implications for the earthquake mechanism, *J. Geophys. Res.* **77,** 6392–6406.

Swanger, H. J., S. M. Day, J. R. Murphy, and R. Guzman (1980). State-of-the art study concerning near-field earthquake ground motion, Nuclear Regulatory Commission Report NUREG/CR-1978, prepared by Systems, Science and Software.

Virieux, J. and R. Madariaga (1982). Dynamic faulting studies by a finite difference method, *Bull. Seism. Soc. Am.* **72,** 345–369.

Wu, F. T. and H. Kanamori (1973). Source mechanism of February 4, 1965, Rat Island earthquake, *J. Geophys. Res.* **78,** 6082–6092.

Wu, F. T., K. C. Thomson, and H. Kuenzler (1972). Stick-slip propagation velocity and seismic source mechanism, *Bull. Seism. Soc. Am.* **62,** 1621–1628.

SYSTEMS, SCIENCE AND SOFTWARE
P.O. BOX 1620
LA JOLLA, CALIFORNIA 92038

Manuscript received 23 December 1981